# Error-State Kalman Filter for Online Evaluation of Ankle Angle

Ahmed Soliman<sup>1</sup>, Guilherme A. Ribeiro<sup>1</sup>, Andres Torres<sup>2</sup>, Mo Rastgaar<sup>1</sup>

Abstract— This paper presents an Error-State Kalman Filter (ESKF) for state estimation in a 2-DOF robotic prosthetic ankle. The filter estimates the ankle angle in inversion-eversion (IE), external-internal (EI), and dorsiflexion-plantarflexion (DP), using measurements from two low-cost magnetic, angular rate, and gravity sensor modules (MARGs), also known as 9-axis Inertial Measurement Units (IMUs). To this end, we transformed raw MARG measurements into body frames and modeled the states and constraints of the 2-DOF robotic prosthesis in an Error State Kalman Filter (ESKF). Experimental tests showed the proposed ESKF provided better results than the Madgwick filter, a commonly used attitude estimator. The proposed filter is developed for ankle prostheses requiring direct angle measurement and can be expanded to an online evaluation of ankle angle in humans.

## I. INTRODUCTION

Robotic lower-limb robotic legs aid amputees in their daily activities, improving their quality of life. Amputees have a slower gait and exert more energy during gait than healthy individuals [1], [2]. This is mainly due to the lack of assistive energy in passive prosthetic legs, unlike human neuromuscular activities [3]. Furthermore, as amputees seek to compensate for the lack of net positive energy in a passive prosthesis, secondary injuries occur in other joints [4]. Thus, robotic lower limb prostheses are required to assist amputees in daily activities.

During walking, the ankle generates torques in inversioneversion (IE), external-internal (EI), and dorsiflexionplantarflexion (DP) directions [5]. Therefore, the control of lower-limb prostheses is a critical topic that has attracted interest from many researchers. Position and effort controllers are applied to the human ankle for rotations in one or two planes of motion, IE and DP. Robotic prosthesis utilizes DC motors to actuate the human ankle in one or two degrees of freedom.

A widely used prosthesis assembly is direct screw and pulley assemblies between the DC motors and the prosthesis foot [3], [6]–[10]. This strategy allows for control of the position of the robotic ankle that rotates while constrained by a revolute joint, tying the shank and foot frames together. DC motors are also assembled remotely from the robotic ankle; motors are connected to the ankle through Bowden cables [11], [12]. Remote assemblies of motors lower the weight of robotic prosthetic legs. When either assembly strategy is used, the ankle

Attitude estimator algorithms are progressively utilized as motion capture algorithms in robotic and human movement studies. Such algorithms commonly use Inertial Measurement Units (IMUs) due to their low cost and portability. Madgwick et al. fused an IMU and magnetic angular rate and gravity (MARG) sensors to estimate orientation using optimized gradient descent. Their estimation results match the performance of a Kalman-based algorithm [14]. Srang et al. fused joint state and Stribeck friction parameter as a discontinuous friction model. For attitude estimation, they used a continuous-discrete unscented Kalman filter for which prediction and correction can be made via unscented transform [15]. Wang et al. estimated the yaw rate, sideslip angle, and vehicle speed of a three-degree-offreedom (TDOF) vehicle. Based on developed vehicle dynamics and a continuous-time-state-space model, a robust cubature Kalman filter is used to estimate the vehicle states [16]. Vitali et al. implemented a robust error-state Kalman filter for estimating IMU orientation. Their filter defined the true state as the sum of a nominal and error state. They validated their work by placing IMU on a coordinate measurement machine (CMM) [17]. Hasan used a low-cost IMU and an eXogenous Kalman Filter to estimate the position and attitude of a four Omni-wheeled ball balancing robot (Ballbot). Hasan combined a Nonlinear Observer (NLO) and a Linearized Kalman Filter (LKF) to achieve non-linear estimation [18].

The team previously designed a 2-DOF robotic prosthesis, where the ankle angle is estimated using an experimentally computed Jacobian relationship between motor angels to ankle angle [11]. The ankle is connected to the drums of the motor

angle is a feedback signal to the control schemes of the robotic ankle prosthesis. Ankle angle is measured using direct and indirect approaches. Direct approaches are made through joint encoders placed on the prosthesis carbon fiber foot or at rotating revolute joints, measuring the rotation of the ankle in DP [3], [10], [12]. Indirect approaches include placing an encoder on motors connected remotely to the ankle using Bowden cables [11], [12]. The displacement of actuators isn't a reliable and accurate measure of the ankle angle due to Bowden cables' flexibility, deflection, and slippage around winch assemblies with motors [13]. Latency issues caused by Bowden cable assemblies also limit the position bandwidth of the ankle prosthesis controller. Slippage in gears, pulleys, and ankle joints causes an error in measuring ankle angle.

<sup>\*</sup>This work was supported by the National Science Foundation (NSF), Grant Number 1921046.

<sup>1.</sup> The authors are with the Polytechnic Institute, Purdue University, West Lafayette, IN 47906 USA (corresponding author e-mail:rastgaar@purdue.edu).

The author is with Mechanical Engineering, Purdue University, West Lafayette, IN 47906 USA.

through a winch assembly of Bowden cables and steel wires. During clinical trials, steel wires momentarily slipped from the winch assembly, causing errors in the trajectory followed by the robotic ankle. The control bandwidth was also limited due to lag caused by the deflection of Bowden cables. In this work, an actual direct reading of the ankle angle in two degrees of freedom is derived independent of motor displacement; to improve the team's previous work. This study uses a strain gauge bridge to detect the heel strike and stance phase and two magnetic, angular rate, and gravity sensor modules (MARGs) as inputs to an Error-State Kalman filter (ESKF) that estimates the shank and foot orientation. The ankle rotation in IE, EI, and DP is computed through the relationship between shank and foot quaternion orientations.

This paper first introduces related studies and research challenges in section I. Then, we briefly discuss the methodology used previously to measure the ankle angle, present in the new 2-MARG setup, strain gauge bridge configuration, and finally, the Error-State Kalman Filter (ESKF) methodologies. Lastly, the results, discussion, and conclusion are presented in Sections III, IV, and V. Section VI shows the availability of data and how the proposed work can be replicated.

## II. METHODS

# A. Indirect ankle angle measurement through Jacobian transformation

The Jacobian relationship between motor angle to ankle angle is computed using a ground truth measurement of the ankle angle fitted against the corresponding motor angle. The ground truth measurement is retrieved using ten optical marker cameras (OMC) (Miqus M5, Qualisys, Sweden) that track the prosthetic shank (pylon) and foot (Fig. 1.a) quaternion orientations ( $q_s$  and  $q_r$  respectively). The 2-DOF ankle oscillates through a 2 Hz sine wave in DP and IE rotations while tracked by the OMC for a duration of two minutes.

The quaternion product ( $\otimes$ ) between the shank quaternion and the inverse foot quaternion equals ankle angle,  $q_{\theta}$ , in quaternion form (Equation 1). Consequently, ankle angle,  $\theta$ , is computed as shown in Equation 2 ([19], chapter 5).  $\theta$  represents ankle angle rotation in IE ( $\theta_{IE}$ ), EI ( $\theta_{EI}$ ), DP ( $\theta_{DP}$ ).

$$q_{\theta} = q_{F}^{-1} \otimes q_{S}$$

$$\theta = \begin{cases} \theta_{IE} \\ \theta_{EI} \\ \theta_{DP} \end{cases} = \begin{cases} atan2 \left( \frac{2(q_{\theta_{0}}, q_{\theta_{1}} + q_{\theta_{2}}, q_{\theta_{3}})}{q_{\theta_{0}}^{2} - q_{\theta_{1}}^{2} - q_{\theta_{2}}^{2} - q_{\theta_{3}}^{2}} \right) \\ asin \left( 2(q_{\theta_{0}}, q_{\theta_{2}} - q_{\theta_{1}}, q_{\theta_{3}}) \right) \\ atan2 \left( \frac{2(q_{\theta_{0}}, q_{\theta_{3}} + q_{\theta_{1}}, q_{\theta_{2}})}{q_{\theta_{0}}^{2} + q_{\theta_{1}}^{2} - q_{\theta_{2}}^{2} - q_{\theta_{3}}^{2}} \right) \end{cases}$$

$$(2)$$

Where  $q_{\theta}$ ,  $q_F$ ,  $q_S \in SO(3)$  and  $\theta \in \mathbb{R}^3$ .

The computed ankle angle ( $\theta_{IE}$  and  $\theta_{DP}$ ) is fitted against the encoder measurement of the motor's angles ( $\phi_1$  and  $\phi_2$ ) using a 1<sup>st</sup> order regression fit as shown in Fig. 2. The linear regression coefficient vectors are the Jacobian relationship between the ankle and motor angels.

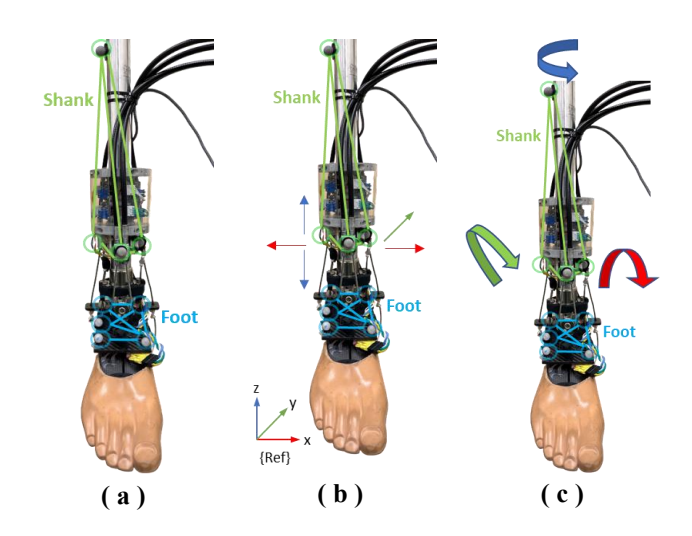


Fig. 1 (a) OMC capture of shank and foot rigid bodies, (b) Accelerometer calibration step while tracked by the OMC, (c) Gyroscope calibration step while tracked by the OMC.

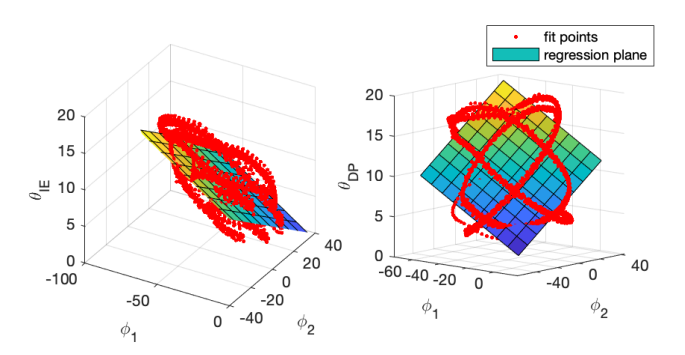


Fig. 2 Regression fit of ankle angle  $(\theta_{IE} \ and \ \theta_{DP})$  against motor angles  $(\phi_1 \ and \ \phi_2)$ .

# B. 2-MARG setup and calibration

Two MARGs (Precision NXP 9-DOF, Adafruit, USA) are rigidly connected to the prosthesis's pylon and spring foot to represent the shank and foot frames, respectively, as shown in Fig. 3, MARGs are sampled at 400 Hz.

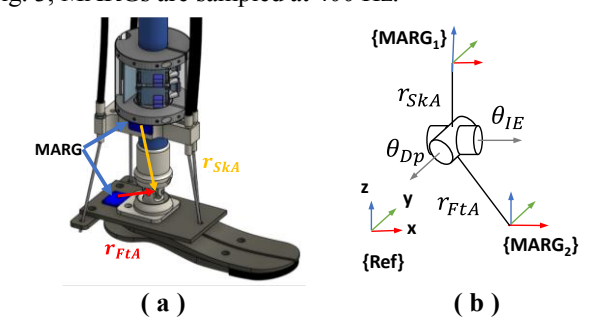


Fig. 3 Assembly of 2 MARGs on the 2-DOF prosthesis. (a) placement of MARG's relative prothesis pylon and carbon fiber foot (b) MARG's tied to universal joints through vectors  $r_{skA}$  and  $r_{FtA}$  respectively.

The angular velocity  $(\omega_t^S)$ , linear acceleration  $(a_t^S)$ , and magnetometer readings  $(m_t^S)$  of the shank are calculated as follows:

$$\omega_t^S = T_{Sw} \omega_t^{MARG_1} - \overline{b_{\omega^{MARG_1}}}$$
 (3)

$$a_t^S = T_{Sa} a_t^{MARG_1} - \overline{b_{a^{MARG_1}}} \tag{4}$$

$$m_t^S = T_{Sm} m_t^{MARG_1} (5)$$

Similarly, the angular velocity  $(\omega_t^F)$ , linear acceleration  $(a_t^F)$  and magnetometer readings  $(m_t^F)$  of the foot are calculated:

$$\omega_t^F = T_{Fw} \omega_t^{MARG_2} - \overline{b_{\omega}^{MARG_2}}$$
 (6)

$$a_t^F = T_{Fa} a_t^{MARG_2} - \overline{b_{a^{MARG_2}}} \tag{7}$$

$$m_t^F = T_{Fm} m_t^{MARG_2} (8)$$

Table 1 ESKF Inputs parameters table

n .	TD 0" ***			
Parameter	Definition			
$\omega_t^{MARG_{1,2}} \in \mathbb{R}^3$	MARGs' raw angular velocities measurements			
$\overline{b_{\omega^{MARG_{1,2}}}} \in \mathbb{R}^3$	Average MARG angular velocity bias			
$a_t^{MARG_{1,2}} \in \mathbb{R}^3$	MARGs' raw linear acceleration measurements			
$\overline{b_{a^{MARG_{1,2}}}} \in \mathbb{R}^3$	Average MARG linear acceleration bias			
$m_t^{MARG_{1,2}} \in \mathbb{R}^3$	MARGs' raw magnetometer measurements			
$T_{Sw}, T_{Sa}, T_{Sm} \in \mathbb{R}^{3\times 3}$	Transformation matrices mapping <i>MARG</i> <sub>1</sub> measurements to OMC shank frame.			
$T_{Fw}, T_{Fa}, T_{Fm} \in \mathbb{R}^{3x3}$	Transformation matrices mapping <i>MARG</i> <sub>2</sub> measurements to OMC foot frame.			
$r_{skA} \in \mathbb{R}^3$	Position of MARG <sub>1</sub> in respect to OMC shank frame			
$r_{FtA} \in \mathbb{R}^3$	Position of MARG <sub>2</sub> in respect to OMC foot frame			

The 2-MARGs are tied together using a universal joint, as shown in Fig. 3.b. The geometrical parameters  $(T_{Sw}, T_{Sa}, T_{Fw}, T_{Fa}, r_{skA}, r_{FtA})$  are estimated using an extrinsic calibration scheme with the OMC (Fig. 1 b, c). The prosthesis's MARGs are excited using an operator in two steps, 1) the operator vigorously moves the prosthesis linearly in the air in all axes motion (x, y, z) to excite the MARGs' accelerometers, then 2) the operator rotates the prosthesis in all axes motion to excite the MARGs' gyroscopes. Each of the MARGs' axes is excited for 10 seconds in each calibration step. The OMC records the shank's and foot's orientation, translation, and body rates in all stages. Measurements from MARG's (  $\omega_t^{MARG_{1,2}}, a_t^{MARG_{1,2}}$ ) are fitted against OMC measurements based on continuous-time batch estimation to provide the

transformation matrices between MARG frames and OMC shank and foot frames [20]. The transformation matrices account for 1) the coordinate frame rotation between the MARGs and the prosthesis shank and foot, respectively, 2) scaling errors, and 3) axis misalignment errors of the MARG [21]. The intrinsic noise parameters of the MARGs (accelerometer, gyroscope) are estimated using Allan Variance analysis [22].  $T_{Sm}$ ,  $T_{Fm}$ , is calculated using the orthogonal averages of  $T_{Sa}$ ,  $T_{Sw}$  and  $T_{Fa}$ ,  $T_{Fw}$  respectively (under MATLAB's rotm2quat and quat2rotm function).

# C. Strain gauge setup and calibration

Four strain gauge bridges (1033-CEA-05-250UWA-350-ND, Digi-Key, USA) were installed on the prosthesis' spring foot to estimate the ground reaction forces and moments. The two spring leaves deflect under the ground reaction forces and torques. The most significant are the vertical force, the DP moment, and the IE moment.

Due to vertical forces and bending moments, the prosthesis foot was modeled as two cantilever beams deflecting along the sagittal plane. Note that the foot is also subjected to frontal and lateral forces and internalexternal moments, but at a much lower



Fig. 4 Strain gauge assembly on prosthesis carbon foot.

significance. Thus, the main forces and moments can be estimated by measuring the deflection of the two cantilevers. In addition, by measuring the surface deflection of the foot in two points, the force and moment in each beam can be estimated.

A calibration procedure was performed to evaluate the DP and IE moments, and the vertical force gave the voltages in the four strain gauge bridges. The prosthesis held the ankle angle to a constant position while the foot was pressed against a force plate sensor (9260AA3, Kistler, Switzerland) to excite the strain gauges to different sensing ranges.

This experiment captured synchronized data from the force plate and the strain gauges at a sampling rate of 400 Hz for approximately one minute. Then, a linear regression model with  $1^{st}$  order and intercept components calculated the vertical force  $(F_y)$  and the DP and IE moments from the strain gauge voltages.

The stance phase is used in the ESKF ankle angle estimation. Stance (S) is identified as a Boolean variable depending on a minimum threshold (k) force. K is empirically tuned through trials (k = 2).

$$S = \begin{cases} 1, & F_y > k \\ 0, & F_y < k \end{cases} \tag{9}$$

# D. Error-State Kalman Filter

The mathematical modeling and filter implementation followed the procedure proposed by Sola [23]. In their method,

the pose of a rigid body was estimated by fusing data from an IMU and an additional generic sensor. In this work, we estimated the pose of two bodies, the foot, and shank, using two MARGs, fusing their magnetometer measurements, and including biomechanical constraints of the foot prosthesis as measurements for the correction step the filter.

The system's nominal states  $(\hat{x})$  were modeled as the orientation of the foot and shank; the position, velocity, accelerometer bias, gyroscopic bias, and magnetometer's hard iron distortion of the two MARGs. Unknown constant parameters were also modeled as states to be estimated by the filter in real-time. These parameters were the magnetic north vector (constraining the x-axis component to zero), and the external-internal (EI) angle of the prosthesis (Equation 2). The EI angle  $(\bar{\theta}_{EI})$  should be equal to zero because the ankle was constructed with a universal joint; However, small errors in the assembly and body definition of the foot and shank cause this angle to be different than zero. The nominal states totaled 42 states.

$$\hat{x} = [p_f, v_f, q_{kf}, ab_f, wb_f, md_F, p_s, v_s, q_{ks}, ab_s, wb_s, md_s, b_v, \overline{m}]^T$$
(10)

Table 2 ESKF nominal states

Parameter	Definition			
$p_f, p_s \in \mathbb{R}^3$	Foot (f) and shank (s) MARGs' position			
$v_f, v_s \in \mathbb{R}^3$	Foot (f) and shank (s) MARGs' velocity			
$q_F, q_S \in SO(3)$	Foot (f) and shank (s) MARGs' quaternion orientation			
$ab_f, ab_s \in \mathbb{R}^3$	Foot (f) and shank (s) MARGs' acceleration bias			
$wb_f$ , $wb_s \in \mathbb{R}^3$	Foot (f) and shank (s) MARGs' gyroscope bias			
$md_f$ , $md_s \in \mathbb{R}^3$	Foot (f) and shank (s) MARGs' magnetometers' hard iron distortion			
$b_y \in \mathbb{R}$	Block yaw (heading of the block)			
$\bar{m} \in \mathbb{R}^3$	Magnetic north vector			

The state equations for the MARG states were modeled in a commonly used indirect approach. The gyroscope and acceleration measurements are used in the state update equation rather than in the measurement equation. This simplifies the modeling of the system, as it eliminates the higher-order rotational differential equations.

The error states  $(\delta \hat{x})$  represented the error for all nominal states as an additive error, except for the orientation variables,

$$\delta \hat{x} = [\delta p_f, \delta v_f, \delta q_{kf}, \delta a b_f, \delta w b_f, \delta m d_F, \\ \delta p_s, \delta v_s, \delta q_{ks}, \delta a b_s, \delta w b_s, \delta m d_s, \delta b_v, \delta \overline{m}]^T$$
(11)

in which a rotational error in the inertial frame was included. The nominal orientation states  $(q_{kf}, q_{ks})$  were represented as unit quaternions with four components, while their respective errors were represented as orientation disturbances with three components  $(\delta q_{kf}, \delta q_{ks})$ .

Ankle angle ( $\theta$ ) is estimated by the filter using the states  $q_F$ ,  $q_S$  as shown in Equations 1 and 2.

The biomechanical constraint equations for the ankle were modeled as

$$p_f + R_{Ft}r_{FtA} - (p_s + R_{Sk}r_{SkA}) = 0 (12)$$

$$\bar{\theta}_{EI} - \operatorname{asin}\left(2(q_{\theta_0}, q_{\theta_2} - q_{\theta_1}, q_{\theta_3})\right) = 0 \tag{13}$$

$$v_1 = 0$$
, if  $S = 1$  (14)

Where,  $R_{Ft}$  and  $R_{Sk}$  are respectively the orientation of the foot and the shank in rotation matrices. These equations constrain the foot and the shank to be connected by a pivot point, the ankle, and to move only in two degrees of freedom ( $\theta_{IE}$  and  $\theta_{DP}$ ) in respect to each other. In Equation (13),  $\bar{\theta}_{EI}$ , is a constant state of the filter, while,  $q_{\theta}$  is calculated as Equation (1). Equation (14) reduces the translational drift of the filter integration by setting the velocity of the foot MARG to zero during the midstance (S). These equations were incorporated into the filter as measurements with additive noise, which are omitted. The noise covariance of the noise was adjusted empirically, considering the mechanical backlash of the universal joint, which would add errors to Equations (12) and (13). While the noise in Equation (14) is mainly originated from the compliance of the foot and ground.

The magnetometers  $(m_t^F \text{ and } m_t^S)$  were incorporated into the measurement equations to reduce the drift of the heading angular error.

$$m_t^F = R_{Ft}^T \overline{m} - m d_f$$
, if  $\left| m_t^{FT} m_t^F - \widehat{m} \right| < \epsilon_m$  (15)

$$m_t^S = R_{SK}^T \overline{m} - md_s$$
, if  $\left| m_t^{S^T} m_t^S - \widehat{m} \right| < \epsilon_m$  (16)

Where,  $\widehat{m}$  is the absolute value of the nominal magnetic field in the area [24],  $\epsilon_m$  is a tolerance for the magnetometer error. These equations are used in the correction step when the measured magnetic field does not deviate substantially from the Earth's magnetic field. If the measurement deviates, there is probably a strong nearby magnetic interference.

Both the update and correction steps of the filter are executed at a rate of 400 Hz. The integration of the nominal and error state equations was performed by a Runge-Kutta (RK4) method and the Euler method [25]. Note that the Euler method is more computationally efficient than the RK4 at the expense of accuracy; However, error dynamics are slow and can be integrated with the Euler method with similar accuracy.

The ESKF is implemented to the prothesis and tested for accuracy in estimating the ankle angle. An un-impaired operator

walks the prosthesis through several gait cycles (lasting a total of 60 seconds), synchronously the prosthesis shank and foot are tracked with the OMC to get a reference measurement of the prosthesis ankle angle (Equations 1&2) as shown in Fig 5. The ESKF estimates the ankle angle in real-time. Fig. 6.a, b. shows

the estimate of the ESKF (solid line) compared to the reference measurement (dashed line). The accuracy of the ESKF is compared to a general attitude estimator's accuracy, the Madgwick filter. The Madgwick filter (Fig. 6.c) was used for evaluation because it has comparable accuracy to generally used attitude estimators such as the Extended Kalman Filter (EKF) [14]. Madgwick filters require a single tuning parameter,  $\beta$ , and the optimal value for  $\beta$  is empirically tuned through a grid search.



Fig. 5 Healthy operator walking 2-DOF prosthetic ankle

# Ankle Angle Estimation Total ESKF estimate **ESKF** ΕI 20 ankle angle [deg] ankle angle [deg] -15 -30 10 12 time [sec] time [sec] (a) (b) Madawick Encoder 10 10 ankle angle [deg] 10 10 10.5 11.5 12 10.5 11.5 12 time [sec] time [sec]

Fig. 6 Estimation of ankle angle by (a) ESKF for whole prosthesis gait trail. (b, c, d) Ankle angle estimate during a 2 second time range. Straight lines represent (b) ESKF, (c) Madgwick filter ( $\beta$ =0.1) (d) encoder-jacobian estimates, dashed lines represent ground truth.

(d)

(c)

The ESKF error is compared to the error of other estimates (Table 3), showing an improvement of the proposed methodology over our previous work (Fig. 6.d) and a comparable attitude estimator.

Table 3 RMSE of different ankle angle estimators

Ankle angle	Estimator			
	ESKF	Madgwick	Encoder	
IE [RMSE °]	0.7724	1.3076	6.9526	
EI [RMSE °]	0.8826	1.0018	-	
DP [RMSE °]	1.3520	1.7640	6.3303	

### IV. DISCUSSION

The proposed filter has implications for studying human kinematics in any environment outside a laboratory, specifically in outdoor environments. Due to the portability and size of MARGs, the ESKF can be easily expanded to study the kinematics of the ankle during outdoor walks of human subjects. We conducted a preliminary study to highlight the potential impacts of acquiring a healthy human subject (23-year-old male, 80 kgs, 165 cm). Two MARGs are tapped into the human subject like the prosthesis configuration (Fig. 7.a).

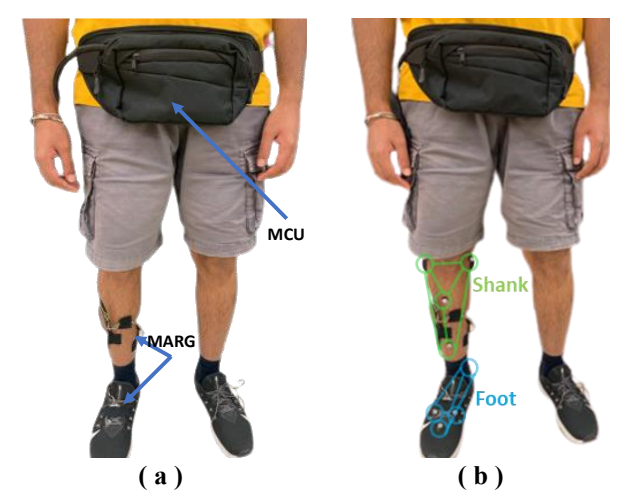


Fig. 7 2-MARG setups for human subject gait analysis during (a) outdoor walk (b) OMC MARGs calibration.

The MARGs are connected to a microcontroller (MCU, Teensy 4.1, PJRC, USA) with a built-in SD card that stores data packets of raw MARG readings (sampled at 400 Hz). MARGs are tapped to the subject using athletic and skin-safe tape; furthermore, wires are twisted and bundled together using wire sleeves; thus, limiting interference with the subject's natural gait. Data is read and stored on the MCU placed inside a fanny pack; the MCU is powered using a small 3.7V Lipo battery. The subject first repeats the MARGs calibration using the OMC (Fig. 7.b), then the subject goes out for a 30-minute outdoor trial. During the 30 minutes, the subject went up and downstairs, walked outdoors, and stood in position to socialize.

At the end of the experiment, data is extracted from the SD card and inputted to the ESKF (offline). There are two differences between the prosthesis and human ESKF: 1) The constraint equation limiting motion in EI for the prosthesis ankle. The human ankle is modeled as a ball joint, allowing

rotation in IE, EI, and DP, thus, the 2-DOF universal joint constraint equation (Equation 13) is removed. 2) Stance phase (S) is identified using changes in the linear acceleration of the foot MARG ( $a_t^F$ ) instead of the prosthesis's strain gauge bridge (Equation 17); this is relevant due to regular spikes in the linear acceleration of the foot MARG during stance phase [26].

$$S = \begin{cases} 1, & \sqrt{\sum (a_t^F)^2} - 9.81 > k \\ 0, & \sqrt{\sum (a_t^F)^2} - 9.81 < k \end{cases}$$
 (17)

Fig 8. Shows the estimate of ankle angle during the subject's 30-minute trial.

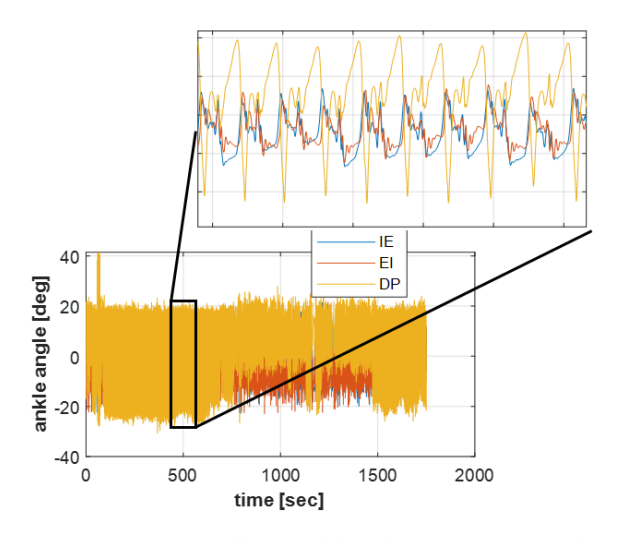


Fig. 8 ESKF estimate of human ankle angle for a 30-minute outdoor trail. Expected cyclic gait pattern observed during gait phase.

## V. CONCLUSION

This paper proposes a new approach for online evaluation of the ankle angle through an ESKF. The implemented ESKF required two low-cost MARGs placed on the shank and spring foot of a 2-DOF robotic prosthesis. MARG calibrations are completed to correct scaling, orientation, and transformation errors of the MARGs. A strain gauge assembly helps detect the stance phase of gait cycles. Corrected MARG readings and a Boolean stance variable are inputs to an ESKF. The EKSF estimated 42 nominal states using Runge-Kutta integration and 40 error states using the Euler integration method. The biomechanics of the prosthesis ankle was considered to correct estimation accuracy. The proposed ESKF can be used for state estimation in prostheses for direct angle measurement at a high sampling rate. The proposed work allowed the team to have a direct ankle angle of a previously designed prosthetic foot, solving issues related to Bowden cable lag and limited controller bandwidth.

Furthermore, the proposed methodology can be extended for ankle angle measurement on human subjects to allow testing of gait cycle kinematics outside of proctored lab space (OMC walkways).

# VI. AVAILABILITY

The MATLAB and C++ deployment of the ESKF section and experimental raw data described in the Methods section is available through (<a href="https://github.com/hirolab/os-eskf">https://github.com/hirolab/os-eskf</a>).

## ACKNOWLEDGMENT

This research was supported by the National Science Foundation (NSF), Grant Number 1921046.

#### REFERENCES

- [1] M. A. Pagliarulo, R. Waters, and H. J. Hislop, "Energy cost of walking of below-knee amputees having no vascular disease," *Phys. Ther.*, vol. 59, no. 5, pp. 538–543, May 1979, doi: 10.1093/ptj/59.5.538.
- [2] W. C. Miller, M. Speechley, and B. Deathe, "The prevalence and risk factors of falling and fear of falling among lower extremity amputees," *Arch. Phys. Med. Rehabil.*, vol. 82, no. 8, pp. 1031–1037, Aug. 2001, doi: 10.1053/apmr.2001.24295.
- [3] A. F. Azocar, L. M. Mooney, L. J. Hargrove, and E. J. Rouse, "Design and Characterization of an Open-Source Robotic Leg Prosthesis," in *2018 7th IEEE International Conference on Biomedical Robotics and Biomechatronics (Biorob)*, Enschede, Aug. 2018, pp. 111–118. doi: 10.1109/BIOROB.2018.8488057.
- [4] J. D. Ventura, A. D. Segal, G. K. Klute, and R. R. Neptune, "Compensatory mechanisms of transtibial amputees during circular turning," *Gait Posture*, vol. 34, no. 3, pp. 307–312, Jul. 2011, doi: 10.1016/j.gaitpost.2011.05.014.
- [5] M. Nordin and V. H. Frankel, *Basic biomechanics of the musculoskeletal system*. Lippincott Williams & Wilkins, 2001.
- [6] D. Quintero, D. J. Villarreal, D. J. Lambert, S. Kapp, and R. D. Gregg, "Continuous-Phase Control of a Powered Knee-Ankle Prosthesis: Amputee Experiments Across Speeds and Inclines," *IEEE Trans. Robot. Publ. IEEE Robot. Autom. Soc.*, vol. 34, no. 3, pp. 686–701, Jun. 2018, doi: 10.1109/TRO.2018.2794536.
- [7] D. Xu, S. Crea, N. Vitiello, and Q. Wang, "Online Estimation of Continuous Gait Phase for Robotic Transtibial Prostheses Based on Adaptive Oscillators," in *2020 IEEE/ASME International Conference on Advanced Intelligent Mechatronics (AIM)*, Boston, MA, USA, Jul. 2020, pp. 1890–1895. doi: 10.1109/AIM43001.2020.9158968.
- [8] J. Zhu, Q. Wang, and L. Wang, "PANTOE 1: Biomechanical design of powered ankle-foot prosthesis with compliant joints and segmented foot," in 2010 IEEE/ASME International Conference on Advanced Intelligent Mechatronics, Jul. 2010, pp. 31–36. doi: 10.1109/AIM.2010.5695879.
- [9] J. K. Hitt, T. G. Sugar, M. Holgate, and R. Bellman, "An active foot-ankle prosthesis with biomechanical energy regeneration," *J. Med. Devices*, vol. 4, no. 1, p. 011003, 2010. [10] E. Bolívar, S. Rezazadeh, T. Summers, and R. D. Gregg, "Robust Optimal Design of Energy Efficient Series Elastic

- Actuators: Application to a Powered Prosthetic Ankle," *ArXiv181204771 Cs*, Feb. 2019, Accessed: May 04, 2020. [Online]. Available: http://arxiv.org/abs/1812.04771
- [11] E. M. Ficanha and M. Rastgaar, "Preliminary design and evaluation of a multi-axis ankle-foot prosthesis," in *5th IEEE RAS/EMBS International Conference on Biomedical Robotics and Biomechatronics*, 2014, pp. 1033–1038.
- [12] J. M. Caputo and S. H. Collins, "A Universal Ankle–Foot Prosthesis Emulator for Human Locomotion Experiments," *J. Biomech. Eng.*, vol. 136, no. 3, p. 035002, Mar. 2014, doi: 10.1115/1.4026225.
- [13] U. Jeong and K.-J. Cho, "A feasibility study on tension control of Bowden-cable based on a dual-wire scheme," in *2017 IEEE International Conference on Robotics and Automation (ICRA)*, Singapore, Singapore, May 2017, pp. 3690–3695. doi: 10.1109/ICRA.2017.7989424.
- [14] S. O. H. Madgwick, A. J. L. Harrison, and R. Vaidyanathan, "Estimation of IMU and MARG orientation using a gradient descent algorithm," in *2011 IEEE International Conference on Rehabilitation Robotics*, Jun. 2011, pp. 1–7. doi: 10.1109/ICORR.2011.5975346.
- [15] S. Srang and M. Yamakita, "Estimation of discontinuous friction using continuous-discrete unscented Kalman filter for adaptive compensation," in *2013 IEEE/ASME International Conference on Advanced Intelligent Mechatronics*, Jul. 2013, pp. 429–435. doi: 10.1109/AIM.2013.6584129.
- [16] Y. Wang, F. Zhang, K. Geng, W. Zhuang, H. Dong, and G. Yin, "Estimation of Vehicle State Using Robust Cubature Kalman Filter," in 2020 IEEE/ASME International Conference on Advanced Intelligent Mechatronics (AIM), Jul. 2020, pp. 1024–1029. doi: 10.1109/AIM43001.2020.9158978.
- [17] R. V. Vitali, R. S. McGinnis, and N. C. Perkins, "Robust Error-State Kalman Filter for Estimating IMU Orientation," *IEEE Sens. J.*, vol. 21, no. 3, pp. 3561–3569, Feb. 2021, doi: 10.1109/JSEN.2020.3026895.
- [18] A. Hasan, "eXogenous Kalman Filter for State Estimation in Autonomous Ball Balancing Robots," in 2020 IEEE/ASME International Conference on Advanced Intelligent Mechatronics (AIM), Jul. 2020, pp. 1522–1527. doi: 10.1109/AIM43001.2020.9158896.
- [19] *Quaternions and Rotation Sequences*. 2002. Accessed: Jan. 31, 2022. [Online]. Available: https://press.princeton.edu/books/paperback/9780691102986/q uaternions-and-rotation-sequences
- [20] P. Furgale, J. Rehder, and R. Siegwart, "Unified temporal and spatial calibration for multi-sensor systems," in *Intelligent Robots and Systems (IROS)*, 2013 IEEE/RSJ International Conference on, 2013, pp. 1280–1286.
- [21] P. Groves, *Principles of GNSS*, *Inertial*, and *Multisensor Integrated Navigation Systems*. 2007.
- [22] "IEEE Standard Specification Format Guide and Test Procedure for Single-Axis Interferometric Fiber Optic Gyros," *IEEE Std 952-1997*, pp. 1–84, Feb. 1998, doi: 10.1109/IEEESTD.1998.86153.
- [23] J. Sola, "Quaternion kinematics for the error-state Kalman filter," *ArXiv Prepr. ArXiv171102508*, 2017.

- [24] N. G. D. Center, "NCEI Geomagnetic Calculators." https://www.ngdc.noaa.gov/geomag/calculators/magcalc.shtml #igrfwmm (accessed Feb. 26, 2022).
- [25] D. F. Griffiths and D. J. Higham, *Numerical Methods for Ordinary Differential Equations*. London: Springer London, 2010. doi: 10.1007/978-0-85729-148-6.
- [26] A. Mansfield and G. M. Lyons, "The use of accelerometry to detect heel contact events for use as a sensor in FES assisted walking," *Med. Eng. Phys.*, vol. 25, no. 10, pp. 879–885, Dec. 2003, doi: 10.1016/S1350-4533(03)00116-4.